ATLAS - An Open-Source TDOA-based Ultra-Wideband Localization System

Janis Tiemann, Fabian Eckermann and Christian Wietfeld

TU Dortmund University, Communication Networks Institute (CNI)

Otto-Hahn-Str. 6, 44227 Dortmund, Germany

{janis.tiemann, fabian.eckermann and christian.wietfeld}@tu-dortmund.de

Abstract—IEEE 802.15.4a Ultra-wideband based wireless positioning has recently gained attention for precise localization. However, the multi-user scalability of those, mostly two-way ranging based, approaches is not considered. Due to the exchange of multiple frames per ranging, two-way ranging has significant downsides in terms of scalability. This paper proposes and validates a novel approach for a multi-user time-difference of arrival based localization system using wireless clock synchronization. The system accuracy is assessed using a complex experiment, covering robotic movement and an optical reference system for comparable results. It is shown, that the accuracies achievable by time-difference of arrival positioning with wireless clock synchronization are comparable to similar two-way ranging based approaches. All raw samples, reference data and processed positions are provided alongside this work.

Keywords—Ultra-wideband (UWB), Time-Difference of Arrival (TDOA), Wireless Clock Synchronization, Wireless Sensor Network, Indoor-Positioning, Open-Source.
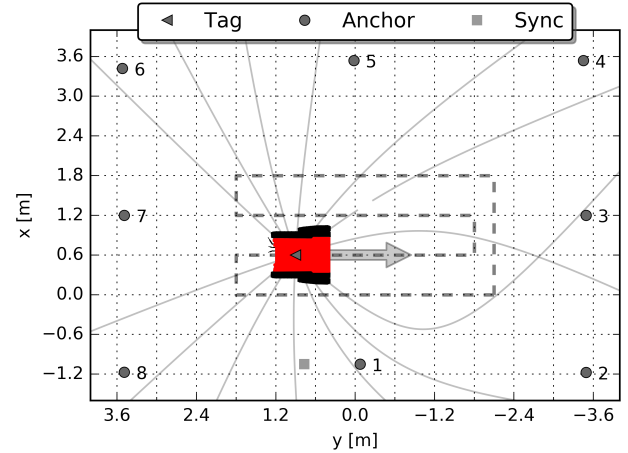
Fig. 1. Top-down illustration of the scenario used for experimental evaluation of the system accuracy. A mobile robot is following a predefined track based on the locations obtained by an optical reference system.

I. INTRODUCTION AND RELATED WORK

Recent developments in ultra-wideband (UWB) transceivers compatible with IEEE 802.15.4a enabled low cost time of arrival (TOA) based localization systems [1]. In [2] a low anchor count system is analyzed experimentally using similar hardware. In those experiments the 90% quantile of the two-dimensional positioning error is in the range of $20\,cm$. In [3] a more complex indoor scenario using multiple anchors was evaluated. Although no detailed statistical evaluation is available, the mean filtered positioning error is denoted under $30\,cm$. Sensor fusion [4] is capable of significantly improving positioning accuracy. However, most of those systems use a single tag, sequentially ranging with a given set of anchor using two-way ranging (TWR) or symmetric double-sided two-way ranging (SDS-TWR) [5]. The exchange of precisely timed frames yields the corresponding round-trip time (RTT) and therefore, substracting the processing times, the propagation duration from the sender to the receiver. However, due to this exchange, the channel is occupied for a significant timespan. Each ranging requires two to four frames, depending on the ranging procedure [6]. Additionally, each transceiver requires time for processing the frames [7]. Since each ranging is conducted with each individual anchor, the channel usage is also multiplied with the amount of anchors. Therefore, TWR is not very capable of scaling to a significant amount of tags [8].

To enable scalable multi-user access, this paper presents a time-difference of arrival (TDOA) based system. Hence the name, TDOA uses the time-differences of the received frame to eliminate the local clock error of the tag. Due to this additional unknown, another anchor is required to estimate the position of the tag. Furthermore, due to the individual drift of the anchor clocks, clock synchronization is required to obtain a common timebase [9]. Therefore the topology of the proposed system is more complex than the topology of TWR based systems. As a result of the additional unknowns, the system accuracy is expected to be lower than the accuracy achievable with TWR based systems.

A comparable system is proposed by [10] to allow for multi-user access. The system topology is inverted compared to the proposed one. Similar to global navigation satellite systems (GNSS), the anchors are transmitting and not receiving. The experiments are conducted using eight anchor nodes and a quadrotor as the mobile platform. The basic results are expected to be very similar to this work.

In the following, the proposed system will be described in detail, covering the individual system components and algorithms. The relevant parts of the software will be provided open source alongside this work for comparability. The accuracy of the proposed system is analyzed using the reference scenario depicted in Fig. 1 and detailed in section III. An optical reference system is used to obtain comparable results. The raw results, sample datasets and reference data of the experimental evaluation are provided alongside this work under a permissive license.
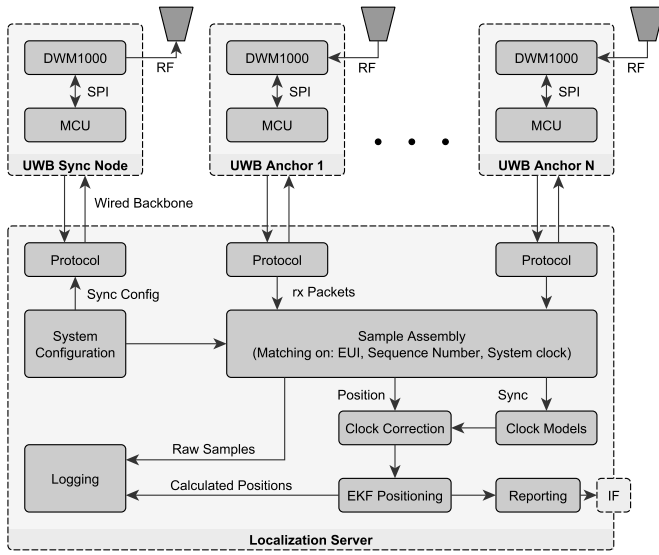
Fig. 2. Topology of the TDOA based localization system. The synchronization node is periodically transmitting a sync packet. The anchor nodes receive this broadcast and communicate the received timestamps to the localization server. Note that the wired backbone is not distributing a common clock.

II. Proposed System Implementation

The ATLAS localization system consists of a set of modular parts. A set of static nodes detailed in section II-A is distributed in the desired localization environment. Those nodes are connected over a wired backbone further described in section II-B to the localization server detailed in section II-C. The system topology is depicted in Fig. 2.

Due to the individual clock drift of each anchor node and the precision needed for accurate TOA measurements, clock synchronization is needed at the receiver nodes. The specific need to enable flexible backbone configuration without timing-critical wiring led to the decision to implement wireless clock synchronization. In this configuration the synchronization node transmits precisely timed periodic synchronization frames at a frequency of 10 Hz. Due to the known periodicity of those frames, a reference clock to estimate the clock drift of the receiving anchors is created.

A. UWB Nodes

The hardware design is based on the *DWM1000* module from *decaWave®* [11]. It is driven by the need for a flexible, integrated and portable solution for scientific purposes. A single microcontroller unit (MCU) was chosen with integrated USB functionality for backbone communication. The hardware design files are provided alongside this work [12].

B. Wired Backbone

The nodes connect to the localization server via a serial connection of any type. The default configuration uses direct connection over a virtual USB serial port. Due to the wireless clock synchronization, the wired backbone is not timing critical. Therefore, configurations with many relays are possible, providing the flexibility to use existing infrastructure.

The backbone protocol is based on the packet structure listed in Tab. I. A binary format was chosen to increase the efficiency of backbone communications. Furthermore, checksumming was added to account for errors during transmission. Received frames are reported to the localization server using the structure listed in Tab. II.

C. Localization Server

The central application used for positioning is the ATLAS Localization Server. The source code of this application is provided alongside our work at [13]. It is based on C++11 using cmake as a build system. Tasks of this central application are:

- Management and configuration of sync nodes and anchors
- Reception, matching and assembly of samples
- Clock correction and positioning
- Logging and reporting of samples and results

As depicted by Fig. 2, the localization server opens connections to the nodes over the wired backbone. Using the binary protocol, described in section II-B, the sync node and the anchors are configured based on unique identifiers of the individual MCUs used by the nodes. After configuration the anchors start reporting received frames with precise TOA timestamps and transmitter extended unique identifier (EUI) to the sample assembly engine. Server-side whitelisting is used to ensure that only tags belonging to the system are processed. The transmitter EUI, the received sequence number and the local server system clock are used to linearize the sequence number. This is neccessary since the transmitted sequence number is limited to 2^8. A sample is complete, when either all anchors received a packet with the same sequence number and transmitter EUI or a local timeout in the lower millisecond range occures dispatching the sample for further processing.

Based on the transmitter EUI, the frame is differentiated if it is a synchronization frame or a positioning frame. The synchronization frames are used to model the individual anchor clocks. Therefore the TOA timestamps need to be linearized and converted first. The TOA timestamp is a 40-bit integer, where one bit corresponds to $1s/(128 \cdot 499.2 \cdot 10^6)$ which is approximately $15.65\,ps$. The local clock overruns every $15.56ps \cdot 2^{40} \approx 17.21s$. Due to this, the TOA timestamps have to be linearized at the localization server for accurate

TABLE I.   Structure of a backbone protocol packet.

type	name	description
uint16_t	pream	Preamble of a binary packet
uint16_t	msgId	Message id of the binary packet
uint16_t	length	Payload length
uint8_t[]	payload	Payload with variable length
uint16_t	checksum	Checksum

TABLE II.   Structure of received frame payload.

type	name	description
uint64_t	txEui	EUI of the transmitting node
uint64_t	rxEui	EUI of the receiving node
uint64_t	rxTs	Precise timestamp of frame reception
uint8_t	seq	Sequence number locally increased by the anchor

clock synchronization. During linearization it is assumed that at least one frame is received in the cycle time.

D. Clock Correction

A clock model is kept for each anchor clock. If a synchronization frame is received, it is used to update the state of the clock model. If a positioning frame is received, that model is used to calculate the corrected TOA with respect to the sync node clock. A simple clock model, based on a clock offset ε and a clock drift $\dot{\varepsilon}$ is used. The reference clock is obtained by the multiplication of the sync sequence number k and the synchronization interval τ_s as shown in (1). For simplification it is assumed, that the synchronization frame sequence number equals the synchronization step.

$$t_{r,k} = k\tau_s \tag{1}$$

At each synchronization step k, the clock offset $\varepsilon_{n,k}$ of an anchor n is calculated using the measured TOA of the synchronization frame $t_{sn,k}$ and the calculated reference TOA $t_{r,k}$ as shown in (2).

$$\varepsilon_{n,k} = t_{sn,k} - t_{r,k} \tag{2}$$

To obtain the clock drift $\dot{\varepsilon}_{n,k}$, the current clock offset is compared to the last offset calculated at the previous timestep $k-1$, see (3).

$$\dot{\varepsilon}_{n,k} = \frac{\varepsilon_{n,k} - \varepsilon_{n,k-1}}{\tau_s} \tag{3}$$

The clock models for each anchor n are used, to extrapolate the clock offset $\varepsilon_{n,i}$ at the reception of a positioning frame i, to correct the measured TOAs $t_{n,i}$ of the positioning frame, see (4).

$$\varepsilon_{n,i} = \varepsilon_{n,k} + \dot{\varepsilon}_{n,k}(t_{n,i} - t_{sn,k}) \tag{4}$$

This extrapolation is necessary, as the drift between the reception of the last synchronization frame and the current positioning frame may have significant influence on the positioning results. The extrapolated errors are then simply subtracted from the measured TOAs to obtain the corrected TOAs.

E. Calibration and Outlier Detection

Early experiments showed static offsets in the TOA measurements of the receivers, similar to the ones observed in [10]. Therefore, the option to initially calibrate the system with a calibration node at a known position was included in the system. Since the position of the node is known, the expected TDOAs may be calculated. Using the difference of the measured TDOA versus the calculated TDOA, the calibration process gradually builds up a calibration offset for each anchor. This offset is later subtracted from the measured TDOAs for the tags.

Furthermore, a basic outlier detection is used to filter erroneous measurements. In a first stage TDOA measurements are filtered that lie outside a threshold of plausibility for the observed area. This is done, comparing the absolute TDOA value to a previously determined threshold based on the area dimensions. However, many outliers are inside of this threshold. Therefore, also the temporal differentiation of the TDOA values per tag and corresponding anchors are tracked individually. If the change is greater than a certain threshold, the corresponding sample is dropped, too. In this work, the absolute threshold is $15\,\mathrm{m}$ and the dynamic is $0.5\,\mathrm{m}$. Future work may include dynamic selection.

F. Positioning Method

The position estimation is based on an extended Kalman filter (EKF). Position estimation through EKF is well known [14] and therefore only briefly described in this work for the sake of completeness. A constant velocity (CV) model is chosen for simplicity, defined by the state vector s_i in (5). The EKF used in this work is three dimensional. For spatial reasons, only the two dimensional version is shown by the equations.

$$s_i = [x, y, \dot{x}, \dot{y}] \tag{5}$$

The special case of TDOA is mainly visible in the observation vector $h(s_i)$ at positioning step i, depicted by (6). The difference of the distance from the reference anchor $\rho_{1,i}$ and anchor n, $\rho_{n,i}$ is corresponding with the time-difference of arrival measured over the speed of light c.

$$h(s_i) = \begin{bmatrix} \rho_{2,i} - \rho_{1,i} \\ \rho_{3,i} - \rho_{1,i} \\ \vdots \\ \rho_{N,i} - \rho_{1,i} \end{bmatrix} = \begin{bmatrix} c(t_{2,i} - \varepsilon_{2,i} - t_{1,i} + \varepsilon_{1,i}) \\ c(t_{3,i} - \varepsilon_{3,i} - t_{1,i} + \varepsilon_{1,i}) \\ \vdots \\ c(t_{N,i} - \varepsilon_{N,i} - t_{1,i} + \varepsilon_{1,i}) \end{bmatrix} \tag{6}$$

The Jacobian $H(\hat{s}_i)$ used to account for the non-linearity of the positioning equations is described in (7).

$$H(\hat{s}_i) = \begin{bmatrix} \frac{\delta h_2(\hat{s}_{i+1})}{\delta x} & \frac{\delta h_2(\hat{s}_{i+1})}{\delta y} & 0 & 0 \\ \frac{\delta h_3(\hat{s}_{i+1})}{\delta x} & \frac{\delta h_3(\hat{s}_{i+1})}{\delta y} & 0 & 0 \\ \vdots & \vdots & \vdots & \vdots \\ \frac{\delta h_N(\hat{s}_{i+1})}{\delta x} & \frac{\delta h_N(\hat{s}_{i+1})}{\delta y} & 0 & 0 \end{bmatrix}_{(N-1)\times 4} \tag{7}$$

Each element of the Jacobian is described by (8) depending on the previously estimated position $[\hat{x}, \hat{y}]$.

$$\frac{\delta h_n(\hat{s}_{i+1})}{\delta x} = \frac{\hat{x} - x_n}{\hat{\rho}_{n,i}} - \frac{\hat{x} - x_1}{\hat{\rho}_{1,i}} \tag{8}$$

Where the estimated euclidean distance $\hat{\rho}_{n,i}$ from anchor n to the estimated tag position is defined in (9).

$$\hat{\rho}_{n,i} = \sqrt{(x_n - \hat{x})^2 - (y_n - \hat{y})^2} \tag{9}$$
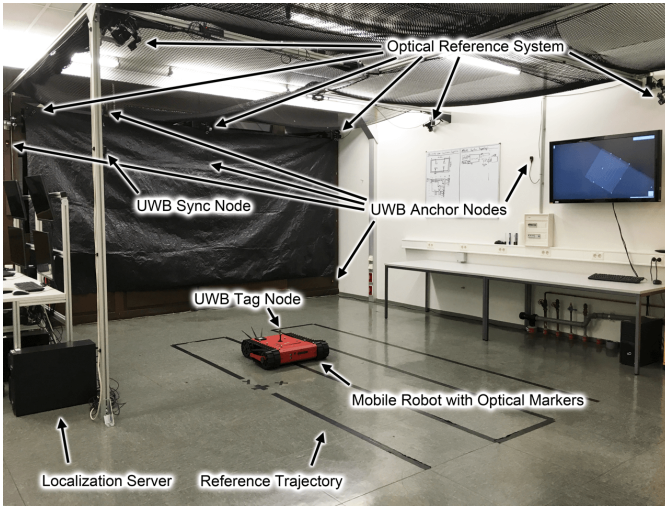
Fig. 3. Experimental setup showing the optical reference system, the UWB synchronization node, the UWB anchor nodes, the localization server, the reference trajectory and the mobile robot equipped with the UWB tag node and the optical reference markers.

III. Experimental Setup

To achieve repeatable results and quantify the accuracy of the proposed approach, a rather complex experiment was set up. As depicted by Fig. 3, a mobile robot follows a predefined trajectory. The robot is mechanically based on the *Dr Robot®* *Jaguar V2* [15]. However, to enable precise control of the actuators, an advanced motor control loop was integrated in the system. The velocity of the tracks are controlled using a cascaded PID track position control loop. The position of the robot is tracked using an *OptiTrack®* motion capture system equipped with eight *Flex 13* cameras [16]. The 6D vehicle position is updated with a frame rate of 120 Hz. The position information is live-streamed to the embedded system on the robot, to allow for precise trajectory following. For statistical relevance, the trajectory was repeated ten times. The motion capture residuals of the individual rays were in the submillimeter range throughout the experiments. The anchor constellation used for the UWB localization is listed in Tab. III. The sync node is placed at $[x_s, y_s, z_s] = [-1.05, 0.77, 1.96]$.

For error analysis, the localization system had to be matched against a reference system. Since the localization system and the optical tracking were executed on different machines, the clocks were synchronized using the network time protocol (NTP). Due to the high frame rate of the motion capture system, and the non-periodic samples of the localization system the temporally closest subset of motion capture frames was chosen for comparison.
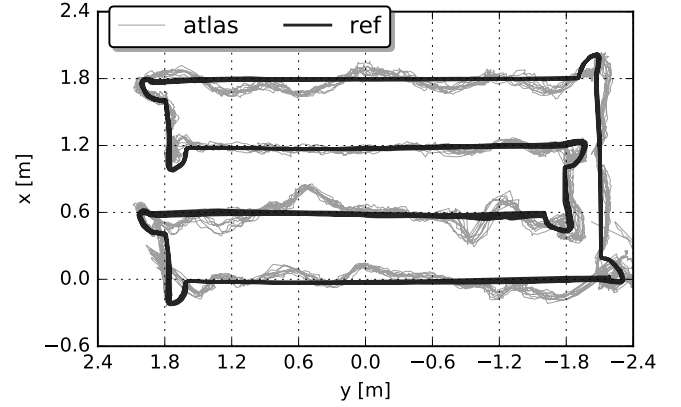

Fig. 4. Top-view of the experimental results. Depicted is the trajectory from the optical reference system as well as the localization results from the ten trajectory repetitions. Note the repeating strong deviations from the reference.

IV. Experimental Results

To increase the repeatability and comparability of the experiments, the raw TOA samples, the localization results and the reference data from the optical reference system are provided alongside this work under a permissive license [17].

A first qualitative horizontal comparison of the localization results and the ground truth is depicted in Fig. 4. The ten repetitions of the experiments are clearly visible. The deviation of the x component appears to be stronger than the y component. However, the deviation appears to have a systematic component. It is assumed that those systematic, repeatable deviations follow a pattern based on the antenna characteristics of the transceivers. Therefore further research may hold the potential for fingerprinting or similar approaches.

A time series of a single trajectory run is depicted in Fig. 5. The y-axis shows good matching with the reference system, which is expected, due to the linear movement. The deviation from the z-axis is stronger due to the chosen anchor constellation optimized for horizontal positioning. The horizontal error χ is under 20 cm most of the time. The strongest horizontal errors resemble the deviations already depicted in Fig. 4.

To assess the effect of calibration discussed in section II-E, the individual errors of the TDOAs in meters of each anchor n compared to the reference anchor $\Delta t_{n,1}$ are depicted in Fig. 6. The TDOA errors are obtained as follows:

$$\Delta t_{n,1} = c(t_n - \varepsilon_n - t_1 + \varepsilon_1) + (\rho_{n,s} - \rho_{1,s}) - (\rho_{n,t} - \rho_{1,t}) \quad (10)$$

The measurements of the optical reference system are used to calculate the euclidean distance between the tag and the n'th anchor $\rho_{n,t}$ as well as the first anchor $\rho_{1,t}$ that acts as the reference for the TDOAs. The distance between each anchor

TABLE III. Positions of the anchors used in the experiments.

anchor	1	2	3	4	5	6	7	8
x [m]	-1.11	-1.17	1.20	3.54	3.54	3.42	1.20	-1.17
y [m]	0.00	-3.49	-3.49	-3.45	0.02	3.52	3.49	3.49
z [m]	2.05	0.29	2.43	2.55	2.08	0.28	2.16	2.17

TABLE IV. Waypoints of the reference trajectory

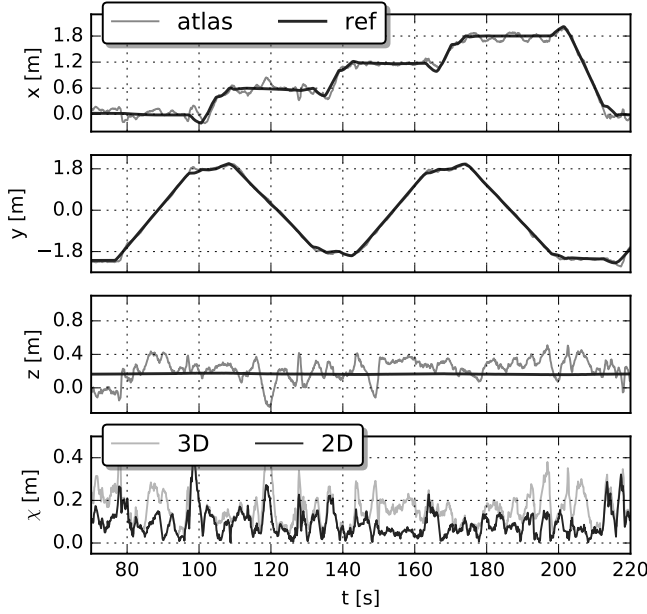| waypoint	1	2	3	4	5	6	7	8
x [m]	-2.10	1.80	1.80	-1.80	-1.80	1.80	1.80	-2.10
y [m]	0.00	0.00	0.60	0.60	1.20	1.20	1.80	1.80

Fig. 5. Time series of a single trajectory run. The individual axes are depicted alongside the euclidean positioning error in the horizontal plane and three dimensional space.
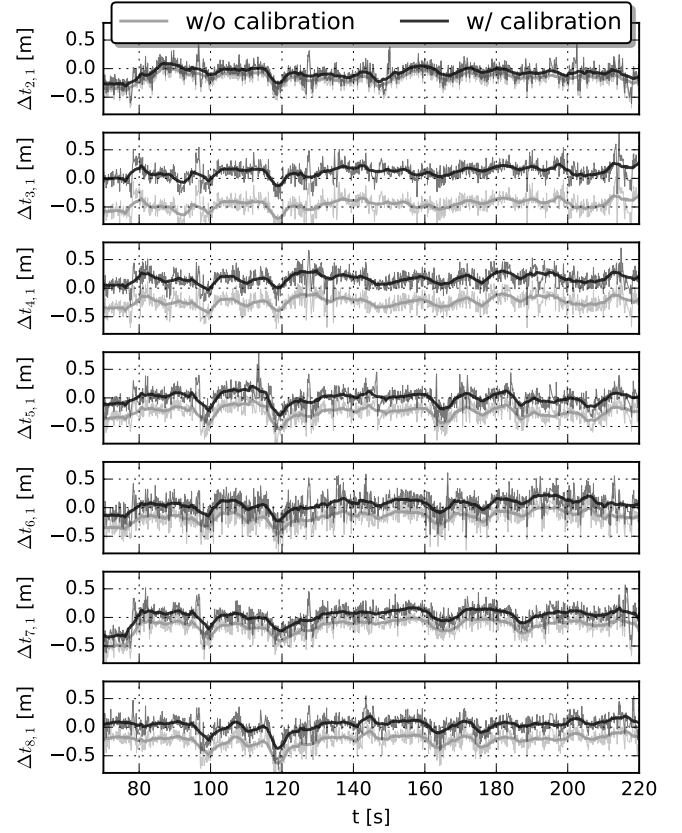

Fig. 6. Time series of the TDOA error $\Delta t_{n,1}$ of a single trajectory run. The TOAs of each anchor are compared to the TOA of the reference anchor. The effect of initial system calibration is visible through error reduction. Note that the overall mean error is not fully mitigated by single point calibration.

and the synchronization node $\rho_{n,s}$ is required as it defines the individual offset of the anchor clock compared to the synchronization node. This offset is introduced by the propagation time from synchronization node to the corresponding anchor. The corrected TDOA $(t_n - \varepsilon_n - t_1 + \varepsilon_1)$ is multiplied with the speed of light in vacuum c to obtain the corresponding distance to the received TDOA. The calibration node is placed at $[x_c, y_c, z_c] = [0.00, 0.00, 0.25]$ at the beginning of the experiment. Once calibrated, the calibration node is removed. Fig. 6 shows the effect of the calibration clearly. Strong offsets, for example at $\Delta t_{3,1}$ are mitigated. However, the calibration is not able to reduce the overall mean TDOA error for all anchors to zero. Therefore, an extensive calibration, using the optical reference system may further improve the system performance for specific cases.

In order to assess the positioning error χ and quantify the system accuracy in this specific configuration, the cumulative distribution functions $\Phi(\chi)$ of the individual axes as well as the two- and three-dimensional configuration are depicted in Fig. 7. For the individual axes, the absolute error is analyzed. The two- and three-dimensional analysis is based on the euclidean error. A statistical evaluation, based on quantiles is listed in Tab. V. The system is performing best along the y axis, showing room for optimization in the anchor constellation.

It should be noted, that the achievable accuracy is strongly dependent on the chosen constellation, the orientation of the anchors, strong multipath effects and other effects. Although many measures to provide comparable results were taken in this work, the achieved results have to be seen in the context of this specific setup. There is still room for improvement.

V. CONCLUSION

This paper presented an alternative to commonly used TWR based UWB localization systems. A system using TDOA
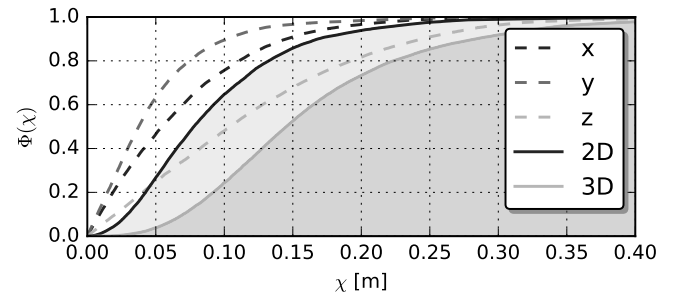

Fig. 7. Cumulative distribution functions $\Phi(\chi)$ of the absolute euclidean errors χ for each axes and the two- and three-dimensional space. Note the difference in accuracy between vertical and horizontal positioning, due to the anchor constellation.

TABLE V. ERROR QUANTILES FOR THE INDIVIDUAL AXES, THE HORIZONTAL PLANE AND THE POSITIONAL SPACE.

	$Q(50\%)$ [m]	$Q(75\%)$ [m]	$Q(90\%)$ [m]	$Q(95\%)$ [m]	$Q(99\%)$ [m]	samples
X	0.054	0.098	0.145	0.180	0.250	13570
Y	0.038	0.066	0.103	0.129	0.228	13570
Z	0.104	0.173	0.244	0.284	0.388	13570
2D	0.078	0.120	0.168	0.212	0.300	13570
3D	0.145	0.205	0.284	0.334	0.456	13570

with receiving anchors and wireless clock synchronization was proposed to improve multi-user scalability. All aspects of the proposed system implementation were covered in detail and the hardware design files as well as the localization server source code were provided alongside this work. The system accuracy was evaluated using a complex experimental setup, combining robotic movement with an optical reference system. The raw TOA samples, positioning results and reference system data are provided to make the results reproducible. A detailed statistical analysis of the system accuracy was provided enabling comparison with similar systems.

Future work may include improving the filtering through sensor fusion, optimizing the channel access for guaranteed quality of service and multi-system clock synchronization. As shown by the results, there is still room for improvement through calibration or other methods assessing the signal properties to achieve elaborated filtering.

REFERENCES

[1] J. Tiemann, F. Schweikowski, and C. Wietfeld. Design of an UWB indoor-positioning system for UAV navigation in GNSS-denied environments. In *Indoor Positioning and Indoor Navigation (IPIN), 2015 International Conference on*, Oct 2015.

[2] W. Chantaweesomboon, C. Suwatthikul, S. Manatrinon, K. Athikulwongse, K. Kaemarungsi, R. Ranron, and P. Suksompong. On performance study of UWB real time locating system. In *2016 7th International Conference of Information and Communication Technology for Embedded Systems (IC-ICTES)*, pages 19–24, Mar 2016.

[3] F. Hartmann, F. Pistorius, A. Lauber, K. Hildenbrand, J. Becker, and W. Stork. Design of an embedded UWB hardware platform for navigation in GPS denied environments. In *Communications and Vehicular Technology in the Benelux (SCVT), 2015 IEEE Symposium on*, pages 1–6, Nov 2015.

[4] H. E. Nyqvist, M. A. Skoglund, G. Hendeby, and F. Gustafsson. Pose estimation using monocular vision and inertial sensors aided with ultra wide band. In *Indoor Positioning and Indoor Navigation (IPIN), 2015 International Conference on*, pages 1–10, Oct 2015.

[5] B. Silva, Z Pang, J. Akerberg, J. Neander, and G. Hancke. Experimental study of UWB-based high precision localization for industrial applications. In *Ultra-WideBand (ICUWB), 2014 IEEE International Conference on*, pages 280–285, Sep 2014.

[6] R. Dalce, A. van den Bossche, and T. Val. An experimental performance study of an original ranging protocol based on an IEEE 802.15.4a UWB testbed. In *2014 IEEE International Conference on Ultra-WideBand (ICUWB)*, pages 7–12, Sep 2014.

[7] R. Dalce, A. van den Bossche, and T. Val. Reducing localisation overhead: A ranging protocol and an enhanced algorithm for UWB-based WSNs. In *2015 IEEE 81st Vehicular Technology Conference (VTC Spring)*, pages 1–5, May 2015.

[8] H. Kim. Performance comparison of asynchronous ranging algorithms. In *Global Telecommunications Conference, 2009. GLOBECOM 2009. IEEE*, pages 1–6, Nov 2009.

[9] C. McElroy, D. Neirynck, and M. McLaughlin. Comparison of Wireless Clock Synchronization Algorithms for Indoor Location Systems. In *Communications Workshops (ICC), 2014 IEEE International Conference on*, pages 157–162, Jun 2014.

[10] A. Ledergerber, M. Hamer, and R. D'Andrea. A robot self-localization system using one-way ultra-wideband communication. In *Intelligent Robots and Systems (IROS), 2015 IEEE/RSJ International Conference on*, pages 3131–3137, Sep 2015.

[11] DecaWave Ltd. *DWM1000 IEEE 802.15.4-2011 UWB Transceiver Module Datasheet 1.0*, 2014.

[12] J. Tiemann. ATLAS UWB node hardware design repository, http://dx.doi.org/10.5281/zenodo.61464. Sep 2016.

[13] J. Tiemann. ATLAS localization server source code repository, http://dx.doi.org/10.5281/zenodo.61465. Sep 2016.

[14] Rafiullah Khan, Francesco Sottile, and Maurizio A. Spirito. Hybrid positioning through extended kalman filter with inertial data fusion. *International Journal of Information and Electronics Engineering*, 3(1):127–131, 1 2013.

[15] Dr Robot. Dr robot jaguar. [Online]. Available: http://jaguar.drrobot.com/specification_V2.asp, Sep 2016.

[16] OptiTrack. Optitrack website. [Online]. Available: http://optitrack.com/, Sep 2016.

[17] J. Tiemann. Raw experimental ATLAS localization, sample and tracking data, http://dx.doi.org/10.5281/zenodo.61335. Sep 2016.